Journal Name

COMMUNICATION

$Ag:BiVO_4$ dendritic Hybrid-architecture for High Energy Density Symmetric Supercapacitors

Received 00th January 20xx,
Accepted 00th January 20xx

DOI: 10.1039/x0xx00000x

www.rsc.org/

Santosh S. Patil[†,a,b] Deepak P. Dubal[†,c] Mohaseen S. Tamboli,[a] Jalindar D. Ambekar,[a] S. S. Kolekar,[b] Pedro Gomez-Romero,[c] Bharat B. Kale*[a] and Deepak R. Patil*[a]*

We demonstrate fabrication of $Ag:BiVO_4$ with a dendritic architecture by template free hydrothermal method. Then, symmetric cells based on $Ag:BiVO_4$ electrodes were assembled which exhibits an extended voltage window up to 1.6 V with excellent energy density of 2.63 mWh/cm^3 (38.43 Wh/kg) and power density of 558 mW/cm^3 (8.1 kW/Kg).

In the recent surge of sustainable energy demand, supercapacitors (SCs) occupy a special niche as novel, environmentally-friendly, low-cost, and high-performance energy storage devices.[1] Supercapacitors have the ability to store charges through double-layer (non-faradaic) and surface redox processes (pseudo-capacitor) thereby achieving high power density and excellent cycling stability but low energy density.[2] So far, different materials such as pseudo-capacitive/faradaic materials (transition metal oxides, polyoxometalates, conducting polymers etc.) and non-faradaic materials (commonly, carbons) are applied as electrode materials for supercapacitors.[3]

Increasing the energy density of supercapacitors is a challenge of the greatest importance. A common approach to enhance the energy density of supercapacitors is the widening of their operational voltage window (since, $E=0.5\ CV^2$). In this context, current research is deeply focused on the fabrication of asymmetric supercapacitors with pseudo-capacitive or faradaic material cathodes and EDLC carbon anodes in aqueous electrolytes.[4] So far carbon-based materials have been adopted as negative electrode materials for hybrid electrodes including activated carbon // $NiCo_2O_4$@MnO_2,[5] graphene foam / polyvinyl alcohol /formaldehyde//activated carbon,[6] etc. Although, asymmetric capacitors show high energy densities and cycling stabilities, the energy density and specific capacitances of carbon anodes are still insufficient to counter balance the electrochemical performance of positive electrode materials. In addition, asymmetric supercapacitors involve a complex balancing of charges from the different electrochemistries in negative and positive electrodes. On the other hand, constructing symmetric capacitors with two identical electrodes can effectively solve this problem; however, this requires strict criteria on the electrodes to give high operation voltage and high-level capacitance with good rate capability. Thus, designing electrode materials with improved storage properties (both specific and volumetric energy and power) to meet the requirements for high-performance energy storage devices is a great challenge.

With this motivation, we have successfully synthesized dendrite-like novel Ag incorporated $BiVO_4$ nano-architecture by simple hydrothermal method. The detailed experimental procedure is given in supporting information S.I. 1. Furthermore, we have proposed a rational design of $Ag:BiVO_4$ based symmetric capacitor which can provide an extended voltage window of 1.6 V. Indeed, this symmetric cell exhibits excellent electrochemical supercapacitive properties due to the incorporation of Ag which further allows fast electron transfer during charge/discharge process.

Fig. 1a shows the comparative X-Ray diffraction patterns of as prepared materials showing crystalline monoclinic phase of pure $BiVO_4$ with lattice constants a = 0.5185 nm, b = 1.1713 nm and c = 0.5102 nm which are in good agreement with literature values (JCPDS card no 014-0688). Additionally, the existence of weak diffraction peak at (37.5^o) was also observed, which corresponds to Ag nanoparticles with cubic crystal structure (JCPDS card no- 04-0783). Fig. 1b depicts the Energy dispersive spectrum of $Ag:BiVO_4$ nanostructure sample confirming the presence of Bi, V, O and Ag elements.

Fig. 2 shows FESEM images of $BiVO_4$ and $Ag:BiVO_4$ samples with corresponding mappings. From Fig. 2a and b, randomly distributed platelet-like particles are observed for $BiVO_4$ sample. Conversely, unique dendrites with leaf-like morphology were observed for $Ag:BiVO_4$ (Fig. 2c and d).

[a] *Centre for Materials for Electronics Technology, Department of Electronics and Information Technology (DeitY), Govt. of India. Pune*
[b] *Analytical Chemistry and Material Science Laboratory, Dept. of Chem., Shivaji University, Kolhapur, India*
[c] *Catalan Institute of Nanoscience and Nanotechnology (ICN2), CSIC and The Barcelona Institute of Science and Technology, Campus UAB, Bellaterra, 08193 Barcelona, Spain Institute of Nanoscience and Nanotechnology, CIN2, ICN2 (CSIC-ICN), Campus UAB, E-08193 Bellaterra, Barcelona, Spain.*
† *These authors contributed equally*

Electronic Supplementary Information (ESI) available: [details of any supplementary information available should be included here]. See DOI: 10.1039/x0xx00000x

Dendritic electrode microstructures are the focus of many researchers due to the remarkable connectivity between the crystals, that enables the construction of high performance electrodes.[7,8] Moreover, the substantial inter-leaf spacing in this particular 3D dendritic structure will provide an easy access for electrolyte ions and hence more electroactive sites as well as small branches will reduce internal resistance.[8, 9]

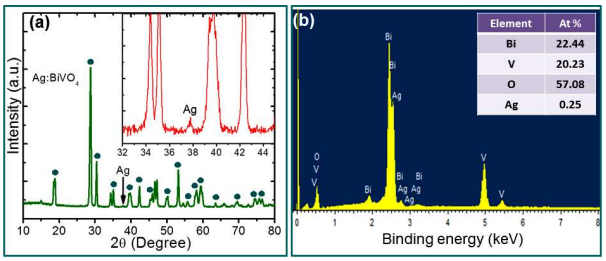

Fig. 1 (a) XRD patterns of $BiVO_4$ and Ag:$BiVO_4$ samples (b) EDAX spectrum of Ag-BiVO4 sample.

Taking a closer look at FESEM image reveals the different features of internal structures to account for formation of dendrite morphology (Fig. 2d). The typical dendrites are formed from two symmetric branches with support of an adequate backbone. The average length of whole single dendrites is around ~ 4-5 µm with widths ranging between 0.5 and 1.5 µm (smaller at the ending side of the dendrite). Every individual branch is further composed of several subunits of different sizes with recognizable boundaries having lengths ranging from 400-600 nm and widths in the range of 100-200 nm attached perpendicular to the backbone to form 3D doubly branched dendrites. The detail reaction and growth mechanism for the evolution of well-defined dendrite morphology via hydrothermal route is given in S.I.2. The additional SEM images have been provided in the supporting information Fig. S.I. 3.

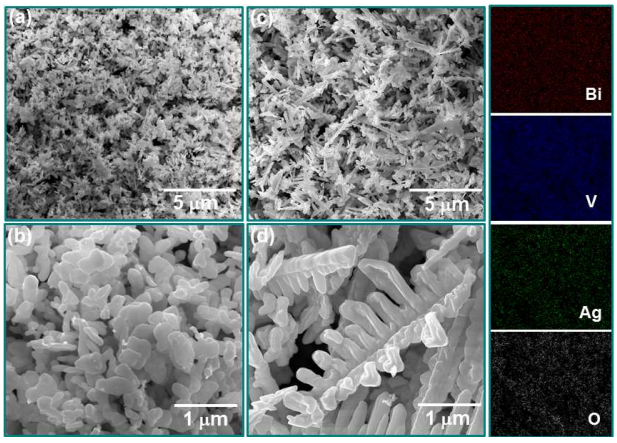

Fig. 2 FESEM micrographs of (a, b) $BiVO_4$ and (c, d) Ag:$BiVO_4$ hybrid microstructures with corresponding elemental mapping images (mapping corresponds to Fig. 2 (c))

The elemental mapping of Ag:$BiVO_4$ dendritic structures shown in Fig. 2 unambiguously confirms the presence of constituent elements Bi, V, Ag and O in the sample.

Further to determine the crystallographic structure and the particle sizes of Ag:$BiVO_4$, FETEM analysis was acquired (Fig. 3). FETEM reveals that the typical dendrites are formed by connecting several submicrons sized subunits on both the sides of single backbone (please also see Fig. S.I. 4). Also, the Ag nanoparticles of size 15-25 nm are in intimate contact with $BiVO_4$. The interface between Ag and $BiVO_4$ is represented by dotted line in TEM images (Fig. 3 (c)). High resolution TEM (HRTEM) image of Ag:$BiVO_4$ (Figure 3c, d) clearly showed two distinct sets of lattice fringes. The uniform lattice fringes with an interplanar spacing of 0.23 nm correspond to the (111) crystallographic plane of Ag while the interplanar spacing of 0.32 nm correspond to (121) crystallographic plane of $BiVO_4$ indicating formation of Ag:$BiVO_4$ hybrid architecture. Inset of Fig. 3c and d depicts the corresponding fast-Fourier-transform (FFT) images.

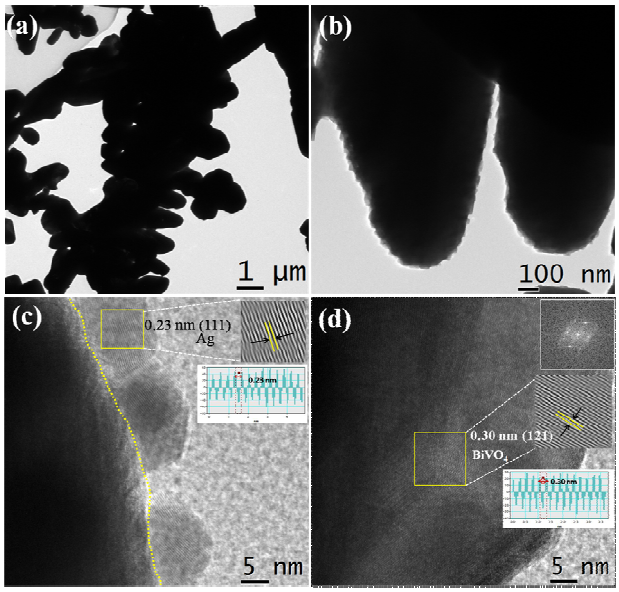

Fig. 3 (a, b) FETEM images of Ag:$BiVO_4$ and (c, d) HRTEM images of Ag and $BiVO_4$ respectively

The obtained Ag:$BiVO_4$ dendritic structure holds several key features such as interlinked connectivity through branched surfaces, propound effect of Ag nanocrystals, improved surface properties and stability. The incorporation of Ag into $BiVO_4$ structure leads to improved charge transfer kinetics on the surface and also facilitates the surface chemical reactions, which is expected to improve specific capacitance through establishing fast electron transfer channels during charge discharge process.[10,11] All these properties are extremely favorable for supercapacitor application.

Considering the unique dendrite structures of the present samples, we investigated the electrochemical performance of $BiVO_4$ and Ag:$BiVO_4$ in 6 M KOH electrolyte. The deviation in a cyclic voltammetry (CV) curve from ideal rectangular shape confirms pseudo-capacitive behavior of both materials as seen in Fig. 4a. It is further interesting to note that, for Ag:$BiVO_4$, the CV curve exhibits relatively high current density with well-defined redox peak, which is attributed to the improved

conductivity of Ag:$BiVO_4$ leading to better ionic and electronic conduction. For the $BiVO_4$ or Ag:$BiVO_4$ electrode, the capacitance mainly arises from the pseudocapacitance due to reversible redox transitions involving the insertion/extraction of protons and/or K^+ ions as well as the transitions between different valence state of V.[12] The possible reaction mechanism is expressed as follows:

$$BiVO_x + yM^+ + ye^- \leftrightarrow V_{2x-y}O_xM_y^{y+} \quad (M^+ = K^+ \text{ or } H^+) \quad (1)$$

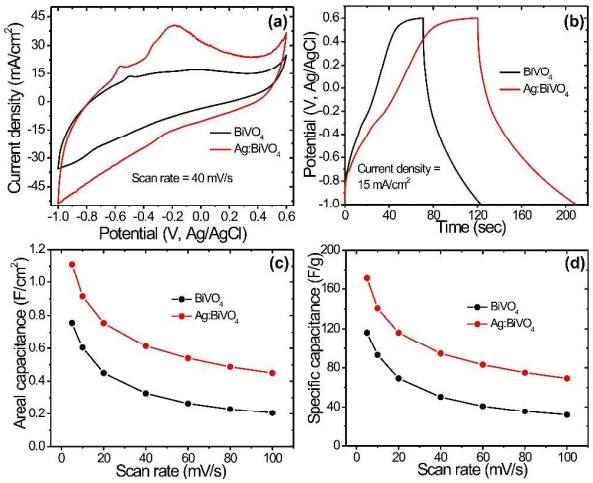

Fig.4 (a) CV curves and (b) Chronopotentiometry curves of $BiVO_4$ and Ag:$BiVO_4$ electrodes at scan rate of 40 mV/s and current density of 15 mA/cm^2, respectively (c) Variation of Areal capacitance of $BiVO_4$ and Ag:$BiVO_4$ nanostructures as a function of scan rates (d) Variation of specific capacitance as a function of scan rates

The CV curves at different scan rates for $BiVO_4$ and Ag:$BiVO_4$ are measured (see Fig. S.I.5). It is worth noting that as scan rate increases the area under the curve increases retaining redox peaks even at high scan rates suggesting excellent rate capability of this material. Fig. 4b shows galvanostatic charge/discharge (CD) curves of $BiVO_4$ and Ag:$BiVO_4$ samples at 15 mA/cm^2. Ag:$BiVO_4$ exhibits higher discharge time than $BiVO_4$ due to low internal resistance of Ag:$BiVO_4$, indicating improved conductivity of Ag:$BiVO_4$ (Fig. S.I.6). The CD curves for $BiVO_4$ and Ag:$BiVO_4$ samples at different current densities from 15 to 40 mA/cm^2 are provided in Fig. S.I.5. The CD curves show symmetrical nature even at high current densities, which further confirms high rate capability of Ag:$BiVO_4$ electrode. The preferable capacitor performance can be attributed to the improved electronic conductivity of the Ag:$BiVO_4$ derived from Ag coating. The above capacitor performance demonstrates that the $BiVO_4$ dendrites coated with Ag nanoparticles exhibit remarkable electrochemical performance for supercapacitor electrodes. The similar kind of improved electrochemical performance owing to improved conductivity of metals oxides coated with polypyrrole (PPy) polymers has been reported earlier.[13, 14] The improved conductivity of Ag:$BiVO_4$ is confirmed by electrochemical impedance measurements (see S.I.6).

For the quantitative analysis of the electrochemical performance, the specific capacitances were derived from the CV measurements. The areal and specific capacitances of $BiVO_4$ and Ag:$BiVO_4$ electrodes at different scan rate are shown in Fig. 4c and d, respectively. The maximum capacitances obtained for $BiVO_4$ and Ag:$BiVO_4$ are 0.75 F/cm^2 (116.3 F/g) and 1.12. F/cm^2 (170 F/g) respectively, at a scan rate of 5 mV/s. The high values of capacitance for Ag:$BiVO_4$ electrode can be attributed to the incorporation of Ag into $BiVO_4$ (improved conductivity) with unique 3D dendrite-like morphology. It is further interesting to note that, the capacitance retention is increased from 26 % to 32 % for Ag:$BiVO_4$ after the increase in scan rate from 5 mV/s to 100 mV/s. Further, the electrochemical stability of $BiVO_4$ and Ag:$BiVO_4$ is measured by charge/discharge cycles at 40 mA/cm^2 as presented in Fig. S.I.6. Both the $BiVO_4$ and Ag:$BiVO_4$ electrodes exhibit capacity retention in the range between 86-88 % after 4000 cycles. All of these results highlight the fact that the addition of Ag to $BiVO_4$ results in enhanced performance by facilitating the faradaic reactions.

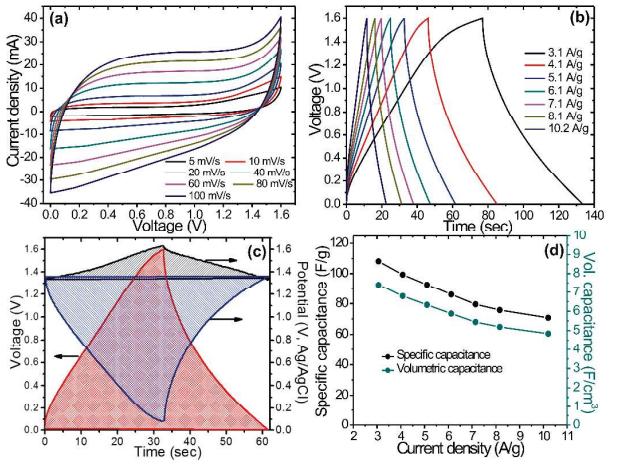

Fig. 5 (a) CV curves of Ag-$BiVO_4$ based symmetric cell at different scanning rates, (b) Galvanostatic charge/discharge (CD) curves of Ag:$BiVO_4$ based symmetric cell at different current densities (c) representative charge discharge cycle at 5.1 A/g for Ag:$BIVO_4$ symmetric cell (d) Variation of specific capacitance and volumetric capacitance at different current densities.

Strikingly, Ag:$BiVO_4$ electrode can work in wider potential window from -1.0 to 0.6 V (vs Ag/AgCl) as shown in Fig 4a and b). Taking advantage of wider potential window, we have assembled a symmetric cell based on Ag:$BiVO_4$ electrodes by sandwiching KOH-soaked separator in between. Thus, the Ag:$BiVO_4$ electrode can be used as both positive as well as negative electrode. Fig. 5a shows cyclic polarization curves of Ag:$BiVO_4$ symmetric cell at various scanning rates. Impressively, the cell can extend voltage window up to 1.6 V, beyond thermodynamic limit of water (1.23 V). It is further interesting to note that the CV curves retain rectangular shape even at high scan rates suggesting good rate capability of electrode materials. Furthermore, the galvanostatic charge/discharge (CD) curves were recorded at various current densities from 3.1 A/g to 10.2 A/g for Ag:$BIVO_4$ symmetric cell (Fig. 5b). It is worth noting that the Ag:$BIVO_4$ symmetric cell shows large voltage window of 1.6 V, which leads to an increased energy density. Fig. 5c shows a representative charge discharge cycle at 5.1 A/g for Ag:$BIVO_4$ symmetric cell.

Each electrode potential limit is also shown (black and blue curves on right Y axis). As expected charging and discharging branches are not straight lines due to the pseudocapacitive contribution. The positive and negative electrodes work in the voltage range: +1.35 to +1.6 V and +1.35V to +0.0 V. Therefore the voltage swing from the negative electrode is much larger than for the positive electrode.

Further, for the quantitative analysis of the electrochemical performance of Ag:$BiVO_4$ symmetric cell, the specific capacitance and volumetric capacitance of Ag:$BiVO_4$ symmetric cell were derived from the CV measurements (S.I.7). Fig. 5d shows the variation of specific capacitance and volumetric capacitance of Ag:$BiVO_4$ symmetric cell as a function of current densities. The Ag:$BiVO_4$ symmetric cell provides a high volumetric capacitance of 7.39 F/cm^3 (108.1 F/g for total mass of active material in both electrodes 4.9 mg/cm^2) at current density of 3.1 A/g. As expected, the capacitance decreases with increase in current density because of diffusion limitation caused by ionic motion of electrolyte. However, the volumetric capacitance at high current density of 7.1 A/g is still considerably high 5.44 F/cm^3 (79.5 F/g). It is noteworthy that the obtained volumetric capacitances are comparatively higher than that of some of the previously reported symmetric as well as asymmetric supercapacitors (see Table S2).[15-17,18] The areal capacitance at different current densities was also calculated and given in Fig. S.I.8. The maximum areal capacitance of 0.73 F/cm^2 was observed at current density of 20 mA/cm^2. The areal capacitance further decreases with increase in current density, consistent with that of volumetric capacitance.

Fig. 6a and b displays the Ragone plots of Ag:$BiVO_4$ symmetric cell. The maximum volumetric energy density of cell is found to be 2.63 mWh/cm^3 (38.43 Wh/kg) at power density of 167 mW/cm^3 (2.44 kW/kg). More interestingly, even at high power density of 558 mW/cm^3 (8.16 kW/kg), Ag:$BiVO_4$ cell exhibits energy density of 1.7 mWh/cm^3 (25.17 Wh/kg), confirming the great potential for application in high performance devices. The enhanced energy and power densities of Ag:$BiVO_4$ symmetric cell are ascribed to high conductivity of Ag:$BiVO_4$ electrode, unique dendrite-like architecture which provide extended voltage window. In comparison to recent novel sodium ion capacitors[19] (energy density of 98 Wh/kg at power density of 2.43 kW/kg), the gravimetric energy density of present Ag:$BiVO_4$ is smaller. However, the observed volumetric energy density is much higher than those of previous reports on symmetric and asymmetric supercapacitors which employed an aqueous electrolyte such as H-TiO_2@MnO_2 //H-TiO_2@C (0.30 mWh/cm^3, 5M LiCl)[18], Co_9S_8//Co_3O_4@RuO_2, (1.21 mWh/cm^3, 3M KOH)[21], VOx//VN (0.61 mWh/cm^3, 5M LiCl)[22], laser-scribed graphene (LSG)//LSG (0.09 mWh/cm^3, 1 M H_3PO_4)[17] demonstrating the remarkable capacitive behavior of Ag:$BiVO_4$/Ag:$BiVO_4$ in aqueous electrolytes.

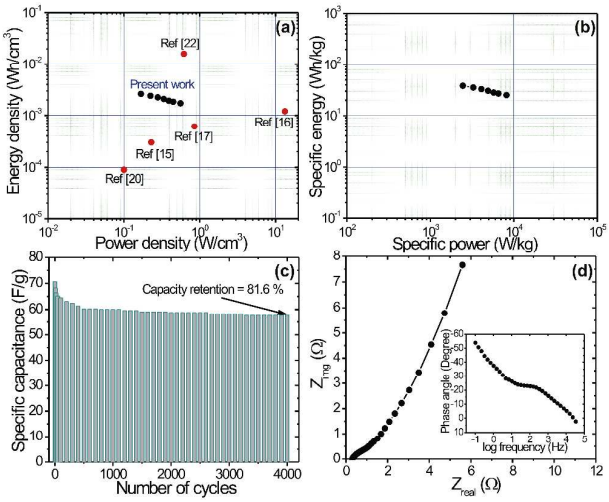

Fig. 6 (a, b) volumetric and gravimetric energy/power densities of Ag:$BiVO_4$ symmetric cell (c) Cycle performance of Ag:$BiVO_4$ symmetric cell, (d) Nyquist plots of Ag:$BiVO_4$ symmetric cell after 4000 cycles (Inset shows plot of phase angle with frequency)

The cycling stability is one of the most important features of high performance supercapacitor device. The stability of Ag:$BiVO_4$ symmetric cell was measured charge/discharge cycles at 10 A/g over 4000 cycles (Fig. 6c). The Ag:$BiVO_4$ symmetric supercapacitor retains 82 % of its initial capacitance after 4000 cycles which is higher than those of earlier reported systems composed of $BiVO_4$ asymmetric capacitor (42% after 200 cycles)[18] and VO_2//VO_2 symmetric supercapacitor (78.7 % after 4500 cycles)[20]. The improved cycling stability might be due to uniquely stable 3D hierarchical dendrite-like structure of Ag:$BiVO_4$. Fig. 6d depicts Nyquist plots of Ag:$BiVO_4$ symmetric cell showing very low ESR value (0.3 Ω) which suggests that the Ag:$BiVO_4$ have very small internal resistance with good ion response at high frequency ranges. The above results indicate that our Ag:$BiVO_4$ hybrid architecture based symmetric supercapacitor exhibits excellent electrochemical supercapacitive properties that could be due to a synergetic effect between noble metal Ag and nano-architectured $BiVO_4$. More importantly, assembling symmetric cells could eliminate the use of complex chemistries usually involved in asymmetric cells (different electrode materials) as well as complication in balancing charge (or mass) of both electrodes. Thus, Ag:$BiVO_4$ symmetric cell outclasses the high-voltage asymmetric counterparts under the same power and represents a noteworthy advance towards high energy density supercapacitors.

In conclusion, a novel Ag:$BiVO_4$ symmetric cell has been successfully fabricated for the first time demonstrating excellent supercapacitive properties. The cell offers an extended voltage window of 1.6 V which further leads to an excellent energy density of 2.63 mWh/cm^3 (38.63 Wh/kg) with high power density of 558 mW/cm^3 (8.1 kW/kg). In addition, notably, this symmetric cell exhibits significantly high volumetric capacitance of 7.39 F/cm^3 and good cycling stability (82 % retention after 4000 cycles). This successful strategy could be applied to the design of new symmetric

supercapacitors using noble metals for doping a variety of high-performing supercapacitor electrode materials.

Notes and References:

1 (a) F. Zhang, T. Zhang, X. Yang, L. Zhang, K. Leng, Y. Huang and Y. Chen, *Energy Environ. Sci.*, 2013, **6**, 1623., (b) D. P. Dubal, J. G. Kim, Y. Kim, R. Holze, C. D. Lokhande, W. B. Kim, *Energy Technol.* **2014**, *2*, 325., (c) D. P. Dubal, P. Gomez-Romero, B. R. Sankapal, R. Holze, *Nano Energy*, **2015**, 11, 377.

2 (a) P. Simon, Y. Gogotsi and B. Dunn, *Science (80-.).*, 2014, **343**, 1210., (b) D. P. Dubal, O. Ayyad, V. Ruiz and P. Gómez-Romero, *Chem. Soc. Rev.*, 2015, **44**, 1777., (c) M. M. Vadiyar, S. C. Bhise, S. K. Patil, S. A. Patil, D. K. Pawar, A. V Ghule, P. S. Patil and S. S. Kolekar, *RSC Adv.*, 2015, **5**, 45935..

3 (a) G. Yu, X. Xie, L. Pan, Z. Bao and Y. Cui, *Nano Energy*, 2013, **2**, 213., (b) J. Suarez-Guevara, V. Ruiz, P. Gomez-Romero, *J. Mater. Chem. A*, 2014, 2, 1014., (c) D. P. Dubal, R. Holze, P. Gomez-Romero, *Sci. Rep.*, 2014, **4**, 7349, (d) D. P. Dubal, J. Suarez-Guevara, D. Tonti, E. Enciso, P. Gomez-Romero, *J. Mater. Chem. A*, 2015, 3, 23483-23492

4 (a) F. Wang, S. Xiao, Y. Hou, C. Hu, L. Liu, Y. Wu, *RSC Adv.,* **2013**, 3, 13059, (b) D. P. Dubal, R. Holze, P. Gomez-Romero, *ChemPlusChem*, 2015, **80**, 944.

5 K. Xu, W. Li, Q. Liu, B. Li, X. Liu, L. An, Z. Chen, R. Zou and J. Hu, *RSC Adv.*, 2014, **2**, 4795..

6 A. Bello, F. Barzegar, D. Momodu, J. Dangbegnon, F. Taghizadeh, M. Fabiane and N. Manyala, *J. Power Sources.*, 2015, **273**, 305..

7 L-X. Ding, F-L. Zheng, J-W. Wang, G-R. Li, Z-L. Wang and Y-X. Tong, *Chem. Commun., 2012, **48**, 1275.*

8 R. Zou, Z. Zhang, M. F. Yuen, J. Hu, C. Lee and W. Zhang, *Sci. Rep.*, 2015, **5**, 1.

9 X. Sun, Z Firdoz, Ying-Xuan, E Li, L Lu, *Nanoscale*, 2013, **5**, 4379.

10 M. Sawangphruk, M. Suksomboon, K. Kongsupornsak, J. Khuntilo, P. Srimuk, Y. Sanguansak, P. Klunbud, P Suktha and P. Chiochan, *J. Mater. Chem. A*, 2013,**1**, 9630.

11 W. Lan, Y. Sun, Y. Chen, J. Wang, G. Tang, W. Dou, Q. Su and E. Xie, *RSC Adv*., 2015,5, 20878.

12 (a) A. M. Engstrom, F. M. Doyle, *J. Power Sources*, 2013, 228, 120, (b) D. H. Nagaraju, Q. Wang, P. Beaujuge, H. N. Alshareef, *J. Mater. Chem. A*, 2014, 2, 17146, (c) X. Lu, M. Yu, T. Zhai, G. Wang, S. Xie, T. Liu, C. Liang, Y. Tong, Y. Li, *Nano Lett.*, 2013, 13, 2628

13 T. Qian, N. Xu, J. Zhou, T. Yang, X. Liu, X. Shen, J. Liang and C. Yan, *J. Mater. Chem. A,* 2015, **3**, 488

14 X. Zhang, X. Zeng, M. Yang and Y. Qi, *ACS Appl. Mater. Interfaces*, 2014, **6**, 1125.

15 X. Lu, M. Yu, G. Wang, T. Zhai, S. Xie , Y. Ling, Y. Tong and Y. Li, *Adv. Mater.* 2013, **25,** 267.

16 J. Xu, Q. Wang, X Wang, Q. Xiang, B. Liang, D. Chen and G. Shen, *ACS Nano*, 2013, **7**, 5453.

17 X. Lu, M. Yu, T. Zhai, G. Wang, S. Xie, T. Liu, C. Liang, Y. Tong, and Y. Li, *Nano Lett.* 2013, **13**, 2628.

18 Z. Khan, S. Bhattu, S. Haram, and D. Khushalani, *RSC Adv.*, 2014, **4**, 17378.

19 F. Wang , X. Wang , Z. Chang , X. Wu , X. Liu , L. Fu, Y. Zhu , Y. Wu and W. Huang, *Adv. Mater*. 2015, **27**, 6962

20 M. F. El-Kady, , V. Strong, , S. Dubin, and R. B. Kaner, *Science*, 2012, **335**, 1326.

21 X-J. Ma, W-B. Zhang, L-B. Kong, Y-C. Luo and L. Kang, *RSC Adv.*, 2015, **5**, 97239.

22 M. Acerce, D. Voiry and M. Chhowalla, *Nat. Nanotech.*, 2015, **10**, 313.

Graphical Abstract

Hydrothermally synthesized Ag:$BiVO_4$ with dendritic structure as an excellent electrode material for symmetric supercapacitors.

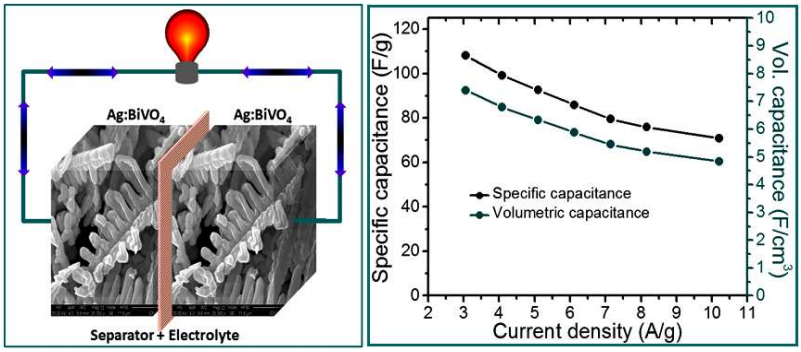

Electronic Supplementary Information

Ag:$BiVO_4$ dendritic Hybrid-architecture for High Energy Density Symmetric Supercapacitors

Santosh S. Patil [†],[a,b] Deepak P. Dubal[†],[c]Mohaseen S. Tamboli,[a] Jalindar Ambekar, [a]

S. S. Kolekar,[b] Pedro Gomez-Romero[c]*, Bharat B. Kale* [a] and Deepak R. Patil*

[a]Centre for Materials for Electronics Technology, Department of Electronics and Information Technology (DeitY), Govt. of India. Pune

[b]Analytical Chemistry and Material Science Laboratory, Dept. of Chem., Shivaji University, Kolhapur, India

[c]Catalan Institute of Nanoscience and Nanotechnology (ICN2), CSIC and The Barcelona Institute of Science and Technology, Campus UAB, Bellaterra, 08193 Barcelona,

Supporting information S. I. 1

Experimental:

Synthesis of Ag:$BiVO_4$ nanostructures:

Bismuth (III) nitrate [$Bi(NO_3)_3.5H_2O$], Ammonium metavanadate [NH_4VO_4] (Qualigen Chemicals Limited), Silver nitrate $AgNO_3$ (SD Fine Chemicals Limited), Ammonia NH_3 (Qualigen Chemicals Limited) and Nitric acid HNO_3 (Fisher Scientific), Ethanol C_2H_5OH (JEBSEN & JESSEN gmbH & Co. Germany) were used as starting materials. All the chemicals were of AR grade and were used without any further purification.

$BiVO_4$, Ag:$BiVO_4$ nanostructures were synthesized by facile solvothermal method. In a typical procedure, initially a mixed solvent was prepared using 5 ml HNO_3, 5 ml C_2H_5OH and 65 ml H_2O. Subsequently, 2.5 mmol of Bi $(NO_3)_3.5H_2O$ and 2.5 mmol of NH_4VO_4 were dissolved separately in each of 35 ml of as prepared solvent. The two solutions were mixed at room temperature under vigorous magnetic stirring and maintained at pH=7 by addition of NH_3. Furthermore, the solution of Ag (1 wt. %) was added dropwise and stirred for 10 min. After being cooled to room temperature naturally, the precipitate was collected and washed with distilled water and ethanol thoroughly, dried at 60^oC for 4 h and used for further characterization. For comparison pure $BiVO_4$ was also prepared were prepared by same method except use of C_2H_5OH in solvent system.

Materials Characterization:

The phase analysis of the samples were performed by X-ray diffraction (XRD) on a Rigaku-Ultima III with CuKα radiation (λ = 1.5418 Å). The surface morphology of as-prepared samples were investigated using the field-emission scanning electron microscopy (FEI Quanta

650F Environmental SEM) attached with an energy-dispersive X-ray spectroscopy (EDS) analyzer to measure the sample composition. Microstructure investigation was conducted using field emission transmission electron microscopy with a JEOL JSM 2200 FS microscope operating at 200 kV.

Electrochemical measurements

In order to check the electrochemical performances, the working electrodeswere prepared by using Doctor Blade method. For this, 85 % of active material (Ag:$BiVO_4$) was mixed with 10 % PVDF as binder and 5 % acetylene black. A few drops of N-Methyl-2-pyrrolidone (NMP, solvent) were added and the mixture was homogenized using a mortar to get a uniform paste. Finally, the paste was applied on commercial flexible carbon cloth which was further used as SCs electrodes. The resultant thin films were then annealed at 180 ^{o}C for two hours in order to remove the binder. The typical mass loading of the electrode material was around 0.5-0.9 mg/cm2. The electrochemical properties were measured using standard three electrode system which contain working electrodes ($BiVO_4$ and Ag:$BiVO_4$), counter electrode (platinum) and reference electrode (Ag/AgCl) in 6 M KOH electrolyte. Symmetric cell was constructed in a 3-way Teflon Swagelok cell using two identical electrodes of Ag:$BiVO_4$ with polypropylene separator sandwiched between them and few drops of 6 M KOH electrolyte. Two channels from potentiostat were connected together in such a way that one channel records voltage between two electrodes (positive and negative) and other channel records potential contributed from positive and negative electrodes with respect to reference electrode. All electrochemical measurements (cyclic voltammetry (CV) and galvanostatic charge-discharge techniques) were carried out using a Biologic VMP3 potentiostat.

Supporting information S. I. 2

Reaction and growth mechanism for Ag:$BiVO_4$ nano-architecture formation

The evolution of well-defined dendrite morphology via hydrothermal route invites the discussion for reaction mechanism and formation mechanism in detail. The plausible reactions taking place in the Ag:$BiVO_4$ hybrid architecture are shown below,

$$Bi(NO_3)_3.5H_2O + HNO_3 + H_2O \rightarrow BiONO_3 + 3\,HNO_3 \quad \ldots\ldots. (1)$$

$$Ag + NH_3 \rightarrow Ag(NH_3)_2^+ \quad \ldots\ldots. (2)$$

$$NH_4VO_3 + BiONO_3 + Ag(NH_3)_2^+ + H_2O \rightarrow Ag{:}BiVO_4 + NH_3 + HNO_3 \quad \ldots\ldots. (3)$$

In a present chemical reaction, the bismuth cations and vanadium anions are provided by the hydration of $BiNO_3.5H_2O$ and NH_4VO_3, respectively. Initially, the hydrolysis of $Bi(NO_3)_3.5H_2O$ takes place and form a soluble $BiONO_3$ which readily react with VO_3^- ions at Ph ~ 6-7 forming pale yellow precipitate of tetragonal $BiVO_4$. During hydrothermal treatment, after getting sufficient thermal energy, the generated $BiVO_4$ nuclei aggregates and converted to highly crystalline form of monoclinic $BiVO_4$ crystals. Meanwhile, the addition of Ag into the reaction medium produces $Ag(NH_3)_2^+$ complex on reaction with NH_3.[1] The formed $Ag(NH_3)_2^+$ complex ions takes sufficient thermal energy to drive-reach the surface of $BiVO_4$ sites wherein gets reduced to Ag by ethanol under high temperature and pressure conditions.[1,2] It is expected that simultaneous nucleation of $BiVO_4$ and Ag might occur which further grow according to self assembly and Ostwald ripening mechanism. It is known that a higher monomer (precursor) concentration in solution generally favors 1D growth whereas the lower monomer concentration favors 3D growth.[3] In the present case, the hydrothermal reaction system with relatively lower reactant concentration, sufficient temperature (180 ^oC) and optimum pH (= 7)

value provides higher chemical potential, and faster ion movement, thereby resulting in formation Ag:$BiVO_4$ hybrid dendritic structures. It is noteworthy that the proper growth of dendrites was observed for Ag:$BiVO_4$ compared to pure $BiVO_4$ sample which might be due to effect of addition of C_2H_5OH as a reducing agent in solvent system, playing a key role on facilitating crystal growth and tailoring the morphology.

From morphology evolution point of view, initially, primary particles starts to aggregate to minimize surface energy, offering driving force for self assembly. The self assembly proceeds by the rotation of particles via Brownian motion and short-range interaction between the particles, causing formation of smaller branches (rod like) that act as building blocks for dendrites. Furthermore, due to prolonged reaction time (24 h) the continuous growth of larger particles are occurred at expense of smaller particles known as Ostwald ripening to form larger subunits or branches to adjust it to achieve a minimum total surface free energy.[3] It is presumed that the an isotropic growth of formed branches along [001] direction is responsible for formation of 3D hierarchical $BiVO_4$ dendritic structures.[4] Thereby, the obtained Ag:$BiVO_4$ dendritic structures preserves several key features of interlinked connectivity through branched surfaces, propound effect of Ag nanocrystals, improved surface properties and stability. Therefore it really sense to examine the performance of this kind of material for energy application.

Supporting information S. I. 3

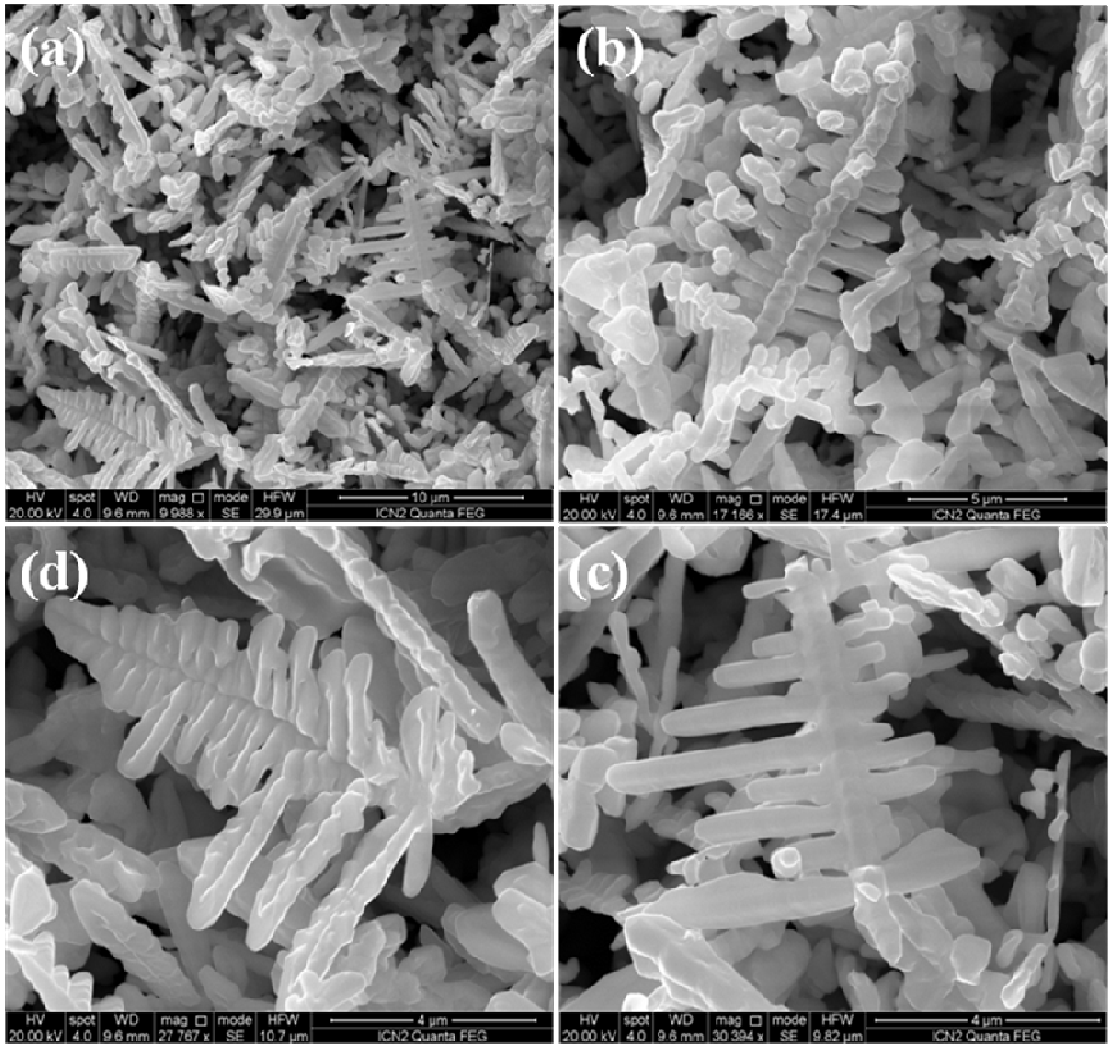

Fig. S.I. 3 FESEM images of Ag:$BiVO_4$ with different magnifications

Supporting information S. I. 4

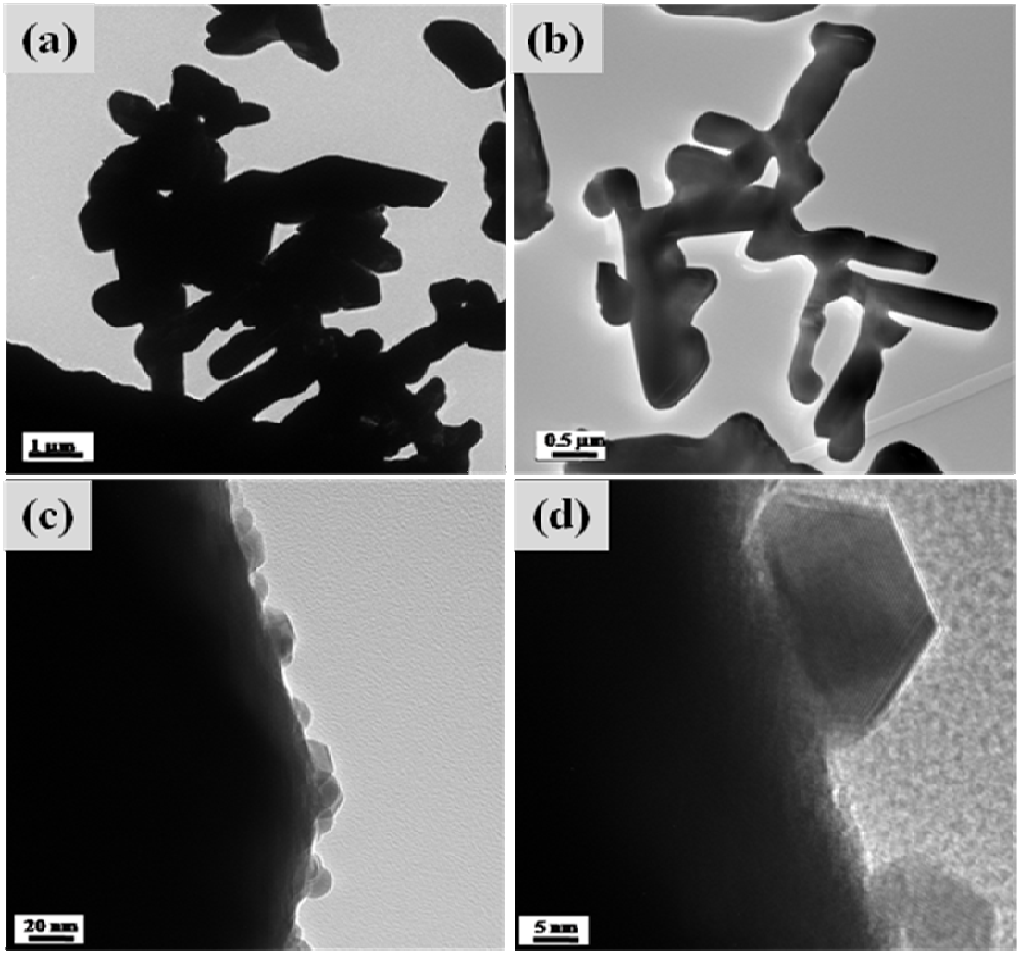

Fig. S.I. 4 FETEM images of Ag:$BiVO_4$ with different magnification

Supporting information S.I. 5

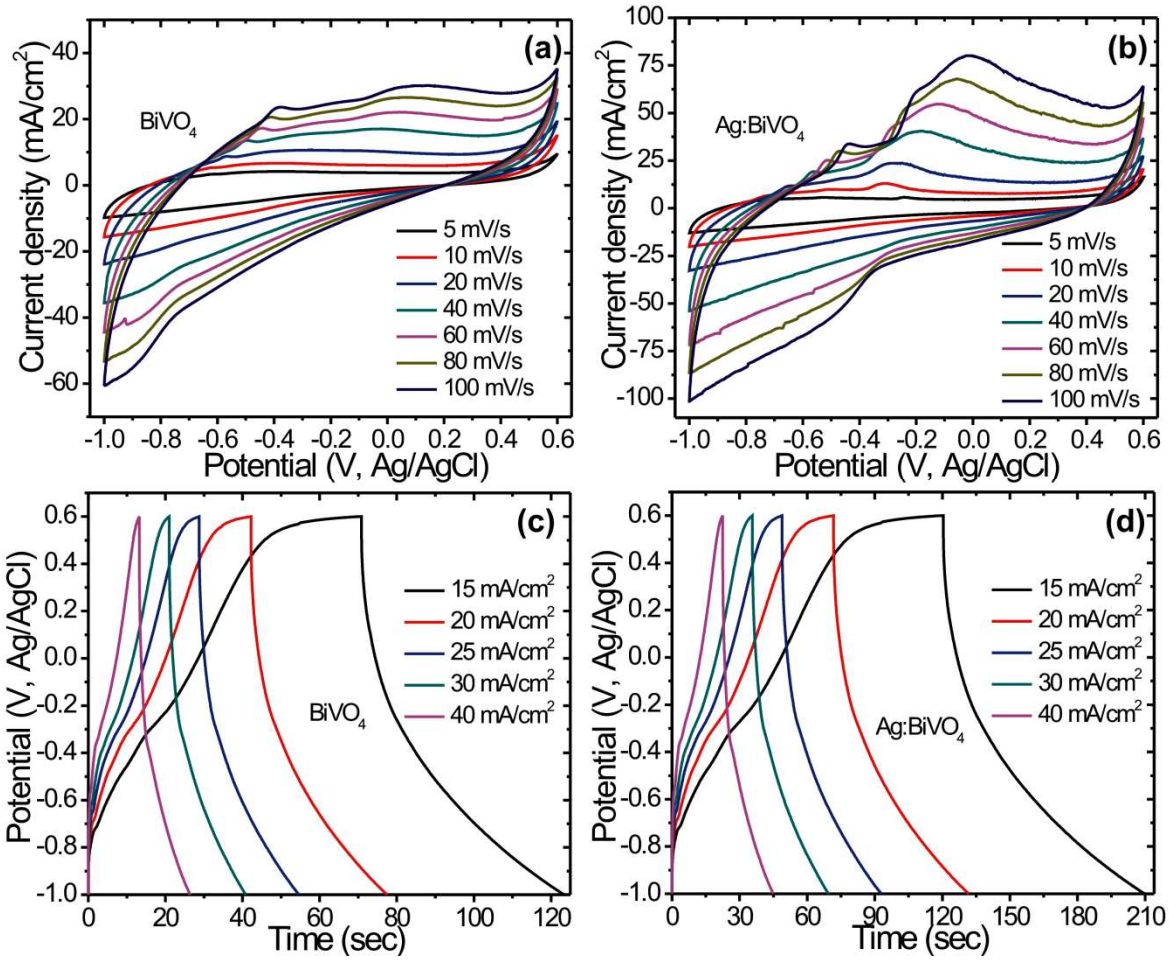

Fig. S. I. 5 Cyclic voltammetry (CV) curves of (a) $BiVO_4$ and (b) Ag:$BiVO_4$ electrodes at different scanning rates and Galvanostatic charge/discharge (CD) curves of (c) $BiVO_4$ and (d) Ag:$BiVO_4$ microstructures at different current densities.

Supporting information S.I. 6

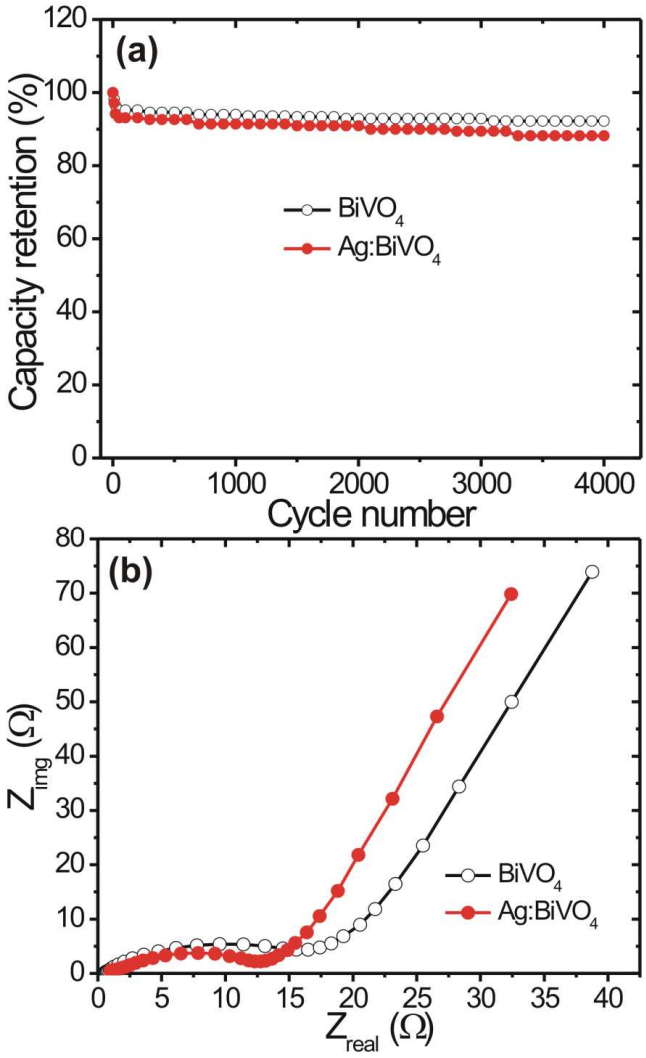

Fig. S.I. 6 Cyclic performance of $BiVO_4$ and Ag:$BiVO_4$ electrodes (b) Nyquist plots of $BiVO_4$ and Ag:$BiVO_4$ electrodes (inset shows the equivalent circuit diagram of Nyquist plots)

Fig. S.I.6 (a) depicts the cycle performance of $BiVO_4$ and Ag-$BiVO_4$ electrodes which showing excellent cycling stability with around 92 % capacity retention after 4000 cycles. The impedance spectra were recorded in order to investigate the bulk solution resistance (R_e), charge transfer resistance (R_{ct}), and Warburg resistance (Z_w) of as synthesized electrode materials. Fig. S.I.6 (b)

displays the Nyquist plots of impedance spectra of the $BiVO_4$ and Ag-$BiVO_4$ with inset showing the equivalent circuit diagram of Nyquist plots. Both the plots showed similar behavior in terms of curve shape (semicircle) except change in the resistance value. The obtained semi circles are due to charge transfer resistance (R_{ct}) which represents how fast the charge transfer takes place at electrode-electrolyte interface. The comparatively lower value of charge transfer resistance (R_{ct}) indicates the improved charge transfer in Ag:$BiVO_4$ hybrid architecture. Further, the small (R_e) value reveals good electrical conductivity of Ag:$BiVO_4$ compared to pristine $BiVO_4$ electrode. This proves that the synergetic effect between Ag and $BiVO_4$ hybrid plays a key role for improving the electrochemical properties by facilitating electronic conduction as well as charge discharge processes. All these results directly reveal the feasibility of using Ag:$BiVO_4$ as a negative electrode for high performance supercapacitor device.

Supporting information S.I. 7

The cell (device) capacitance (C) and volumetric capacitance of the symmetric devices were calculated from their CVs according to the following equation:

$$C_{cell} = \frac{Q}{\Delta V} \quad \text{.....(1)}$$

$$C_A = \frac{Q}{A\,x\,\Delta V} \quad \text{..... (2)}$$

where, C_A and C_V are areal and volumetric capacitances, respectively. Q(C) is the average charge during the charging and discharging process, V is the volume (cm^3) of the whole device (The area and thickness of our symmetric cells is about 0.785cm^2(Area, $A=\pi r^2$, $3.14\times(0.5)^2$) and 0.088 cm. Hence, the whole volume of device is about 0.069 cm^3, ΔV (V) is the voltage window. It is worth mentioning that the volumetric capacitances were calculated taking into account the volume of the device stack. This includes the active material, the flexible substrate and the separator with electrolyte.

Alternatively, the cell capacitance (C_{cell}), areal (C_A) and volumetric (C_V) capacitance of the electrode (C_V) was estimated from the slope of the discharge curve using the following equations:

$$C_{cell} = \frac{Ix\Delta t}{\Delta V} \quad \text{..... (3)}$$

$$C_A = \frac{Ix\Delta t}{A\,x\,\Delta V} \text{ and } \quad Cv = \frac{Ix\Delta t}{V\,x\,\Delta V} \quad \text{..... (4)}$$

Where I is the applied current, V is the volume (cm^3) of the whole device (the whole volume of our device is about 0.069 cm3), Δt is the discharging time, ΔV (V) is the voltage window.

Volumetric energy (E, Wh/cm3) and power density (P, W/cm) of the devices were obtained from the following equations:

$$E = \frac{1}{2 \times 3600} Cv \Delta V^2$$

$$P = \frac{3600 \times E}{\Delta t}$$

where*E* (Wh/cm^3*)* is the energy density, *CV* is the volumetric capacitance obtained from Equation (5) and *ΔV* (V) is the voltage window, P (W/cm3) is the power density.

Supporting information S.I. 8

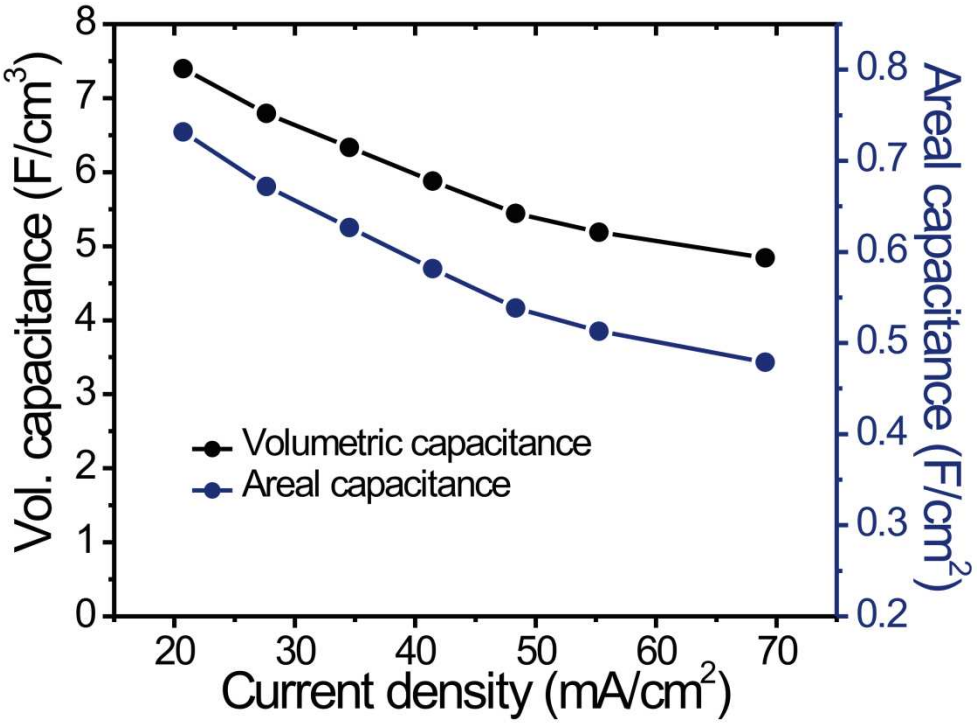

Fig. S.I. 8 Variation of Volumetric capacitance and Areal capacitance with current density of Ag:$BiVO_4$/Ag:$BiVO_4$ symmetric supercapacitors

Table S1: Electrochemical properties of Ag:$BiVO_4$/Ag:$BiVO_4$ symmetric supercapacitors in 6 M KOH electrolyte

Current density (A/g)	Discharge time (sec)	Capacitance		Specific energy	
		Volumetric (F/cm^3)	Gravimetric (F/g)	Volumetric (mWh/cm^3)	Gravimetric (Wh/kg)
3.1	56.5	7.39	108.1	2.63	38.43
4.1	38.92	6.79	99.2	2.41	35.30
5.1	29.04	6.33	92.6	2.25	32.92
6.1	22.46	5.88	85.9	2.09	30.55
7.1	17.82	5.44	79.5	1.93	28.285

Table S2: Comparison of Supercapacitor values of Transition Metal Oxide (TMOs) based electrodes

Electrode	Device	Electrolyte	Volumetric capacitance	Max. Vol. Energy Density at power density	Reference
Ag:$BiVO_4$	Symmetric	6M KOH	7.39 F/cm^3	2.63 mWh cm^{-3} at 0.558 W cm^{-3}	Present work
H-TiO_2 @MnO_2 //H-TiO_2@C	Asymmetric	5 M LiCl	0.68 F/cm^3	0.30 mWh cm^{-3} at 0.23 W cm^{-3}	5
Co_9S_8//Co_3O_4 @RuO_2	Asymmetric	3M KOH	3.42 F/cm^3	1.21 mWh cm^{-3} at 13.29 W cm^{-3}	6
VO_x//VN	Asymmetric	5M LiCl electrolyte	1.35 F/cm^3	0.61 mWh cm^{-3} at 0.85 W cm^{-3}	7
MoS_2	Asymmetric	0.5 M Na_2SO_4	-	0.016 Wh cm^{-3} at 0.62 W cm^{-3}	8
laser-scribed graphene(LSG) //LSG	Symmetric	1.0 M H_3PO_4	0.42 F/cm^3	0.09 mWh cm^{-3}at 0.1 W cm^{-3}	9

References:

1. S. S. Warule, N. S. Choudhari, R. T. Khare, J. D. Ambekar Kale, B. B. Kale and M. A. More, *CrystEngComm.*, 2013, **15**, 7475.
2. Y. Zheng, L. Zheng, Y. Zhan, X. Lin, Q. Zheng and K. Wei, *Inorg. Chem.* 2007, **46**, 6980.
3. R. P. Panmand, R. H. Patil, B. B. Kale, L. K. Nikam, M. V. Kulkarni, D. K. Thombre, W. N. Gade and S. W. Gosavi, *RSC Adv.,* 2014, **4**, 4586.
4. L. Zhou, W. Wang and H. Xu, Cryst. *Growth Des.*, 2008, **8**, 728.
5. X. Lu, M. Yu, G. Wang, T. Zhai, S. Xie , Y. Ling, Y. Tong, and Y. Li, *Adv. Mater.* 2013, **25**, 267.
6. J. Xu, Q. Wang, X Wang, Q. Xiang, B. Liang, D. Chen and G. Shen, *ACS Nano*, 2013 **7**, 5453.
7. X. Lu, M. Yu, T. Zhai, G. Wang, S. Xie, T. Liu, C. Liang, Y. Tong and Y. Li, *Nano Lett.* 2013, **13**, 2628.
8. M. Acerce, D. Voiry and M. Chhowalla, *Nat. Nanotech.*, 2015, **10**, 313.
9. M. F. El-Kady, , V. Strong, , S.Dubin and R. B. Kaner, *Science*, 2012, **335**, 1326.

Journal Name

COMMUNICATION

Ag:$BiVO_4$ dendritic Hybrid-architecture for High Energy Density Symmetric Supercapacitors

Received 00th January 20xx,
Accepted 00th January 20xx

DOI: 10.1039/x0xx00000x

www.rsc.org/

Santosh S. Patil[†,a,b] *Deepak P. Dubal*[†,c] *Mohaseen S. Tamboli,*[a] *Jalindar D. Ambekar,*[a] *S. S. Kolekar,*[b] *Pedro Gomez-Romero,*[*c] *Bharat B. Kale*[*a] *and Deepak R. Patil*[*,a]

We demonstrate fabrication of Ag:$BiVO_4$ with a dendritic architecture by template free hydrothermal method. Then, symmetric cells based on Ag:$BiVO_4$ electrodes were assembled which exhibits an extended voltage window up to 1.6 V with excellent energy density of 2.63 mWh/cm^3 (38.43 Wh/kg) and power density of 558 mW/cm^3 (8.1 kW/Kg).

In the recent surge of sustainable energy demand, supercapacitors (SCs) occupy a special niche as novel, environmentally-friendly, low-cost, and high-performance energy storage devices.[1] Supercapacitors have the ability to store charges through double-layer (non-faradaic) and surface redox processes (pseudo-capacitor) thereby achieving high power density and excellent cycling stability but low energy density.[2] So far, different materials such as pseudo-capacitive/faradaic materials (transition metal oxides, polyoxometalates, conducting polymers etc.) and non-faradaic materials (commonly, carbons) are applied as electrode materials for supercapacitors.[3]

Increasing the energy density of supercapacitors is a challenge of the greatest importance. A common approach to enhance the energy density of supercapacitors is the widening of their operational voltage window (since, E=0.5 CV^2). In this context, current research is deeply focused on the fabrication of asymmetric supercapacitors with pseudo-capacitive or faradaic material cathodes and EDLC carbon anodes in aqueous electrolytes.[4] So far carbon-based materials have been adopted as negative electrode materials for hybrid electrodes including activated carbon // $NiCo_2O_4$@MnO_2,[5] graphene foam / polyvinyl alcohol /formaldehyde//activated carbon,[6] etc. Although, asymmetric capacitors show high energy densities and cycling stabilities, the energy density and specific capacitances of carbon anodes are still insufficient to counter balance the electrochemical performance of positive electrode materials. In addition, asymmetric supercapacitors involve a complex balancing of charges from the different electrochemistries in negative and positive electrodes. On the other hand, constructing symmetric capacitors with two identical electrodes can effectively solve this problem; however, this requires strict criteria on the electrodes to give high operation voltage and high-level capacitance with good rate capability. Thus, designing electrode materials with improved storage properties (both specific and volumetric energy and power) to meet the requirements for high-performance energy storage devices is a great challenge.

With this motivation, we have successfully synthesized dendrite-like novel Ag incorporated $BiVO_4$ nano-architecture by simple hydrothermal method. The detailed experimental procedure is given in supporting information S.I. 1. Furthermore, we have proposed a rational design of Ag:$BiVO_4$ based symmetric capacitor which can provide an extended voltage window of 1.6 V. Indeed, this symmetric cell exhibits excellent electrochemical supercapacitive properties due to the incorporation of Ag which further allows fast electron transfer during charge/discharge process.

Fig. 1a shows the comparative X-Ray diffraction patterns of as prepared materials showing crystalline monoclinic phase of pure $BiVO_4$ with lattice constants a = 0.5185 nm, b = 1.1713 nm and c = 0.5102 nm which are in good agreement with literature values (JCPDS card no 014-0688). Additionally, the existence of weak diffraction peak at (37.5^o) was also observed, which corresponds to Ag nanoparticles with cubic crystal structure (JCPDS card no- 04-0783). Fig. 1b depicts the Energy dispersive spectrum of Ag:$BiVO_4$ nanostructure sample confirming the presence of Bi, V, O and Ag elements.

Fig. 2 shows FESEM images of $BiVO_4$ and Ag:$BiVO_4$ samples with corresponding mappings. From Fig. 2a and b, randomly distributed platelet-like particles are observed for $BiVO_4$ sample. Conversely, unique dendrites with leaf-like morphology were observed for Ag:$BiVO_4$ (Fig. 2c and d).

[a.] *Centre for Materials for Electronics Technology, Department of Electronics and Information Technology (DeitY), Govt. of India. Pune*
[b.] *Analytical Chemistry and Material Science Laboratory, Dept. of Chem., Shivaji University, Kolhapur, India*
[c.] *Catalan Institute of Nanoscience and Nanotechnology (ICN2), CSIC and The Barcelona Institute of Science and Technology, Campus UAB, Bellaterra, 08193 Barcelona, Spain Institute of Nanoscience and Nanotechnology, CIN2, ICN2 (CSIC-ICN), Campus UAB, E-08193 Bellaterra, Barcelona, Spain.*
† These authors contributed equally
Electronic Supplementary Information (ESI) available: [details of any supplementary information available should be included here]. See DOI: 10.1039/x0xx00000x

Dendritic electrode microstructures are the focus of many researchers due to the remarkable connectivity between the crystals, that enables the construction of high performance electrodes.[7,8] Moreover, the substantial inter-leaf spacing in this particular 3D dendritic structure will provide an easy access for electrolyte ions and hence more electroactive sites as well as small branches will reduce internal resistance.[8, 9]

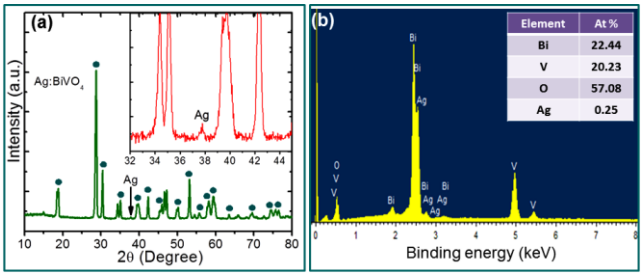

Fig. 1 (a) XRD patterns of $BiVO_4$ and Ag:$BiVO_4$ samples (b) EDAX spectrum of Ag-BiVO4 sample.

Taking a closer look at FESEM image reveals the different features of internal structures to account for formation of dendrite morphology (Fig. 2d). The typical dendrites are formed from two symmetric branches with support of an adequate backbone. The average length of whole single dendrites is around ~ 4-5 µm with widths ranging between 0.5 and 1.5 µm (smaller at the ending side of the dendrite). Every individual branch is further composed of several subunits of different sizes with recognizable boundaries having lengths ranging from 400-600 nm and widths in the range of 100-200 nm attached perpendicular to the backbone to form 3D doubly branched dendrites. The detail reaction and growth mechanism for the evolution of well-defined dendrite morphology via hydrothermal route is given in S.I.2. The additional SEM images have been provided in the supporting information Fig. S.I. 3.

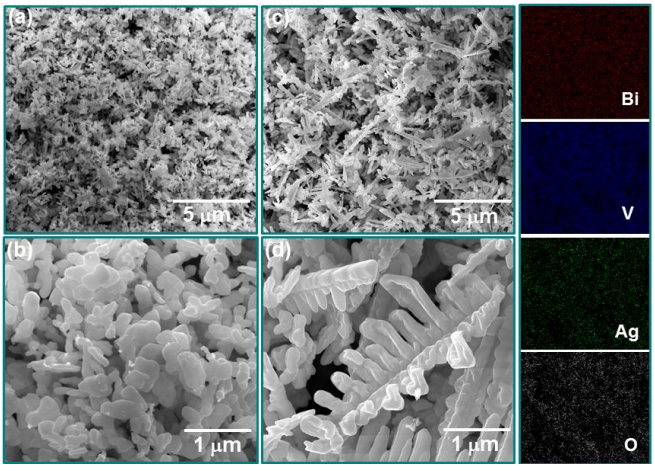

Fig. 2 FESEM micrographs of (a, b) $BiVO_4$ and (c, d) Ag:$BiVO_4$ hybrid microstructures with corresponding elemental mapping images (mapping corresponds to Fig. 2 (c))

The elemental mapping of Ag:$BiVO_4$ dendritic structures shown in Fig. 2 unambiguously confirms the presence of constituent elements Bi, V, Ag and O in the sample.

Further to determine the crystallographic structure and the particle sizes of Ag:$BiVO_4$, FETEM analysis was acquired (Fig. 3). FETEM reveals that the typical dendrites are formed by connecting several submicrons sized subunits on both the sides of single backbone (please also see Fig. S.I. 4). Also, the Ag nanoparticles of size 15-25 nm are in intimate contact with $BiVO_4$. The interface between Ag and $BiVO_4$ is represented by dotted line in TEM images (Fig. 3 (c)). High resolution TEM (HRTEM) image of Ag:$BiVO_4$ (Figure 3c, d) clearly showed two distinct sets of lattice fringes. The uniform lattice fringes with an interplanar spacing of 0.23 nm correspond to the (111) crystallographic plane of Ag while the interplanar spacing of 0.32 nm correspond to (121) crystallographic plane of $BiVO_4$ indicating formation of Ag:$BiVO_4$ hybrid architecture. Inset of Fig. 3c and d depicts the corresponding fast-Fourier-transform (FFT) images.

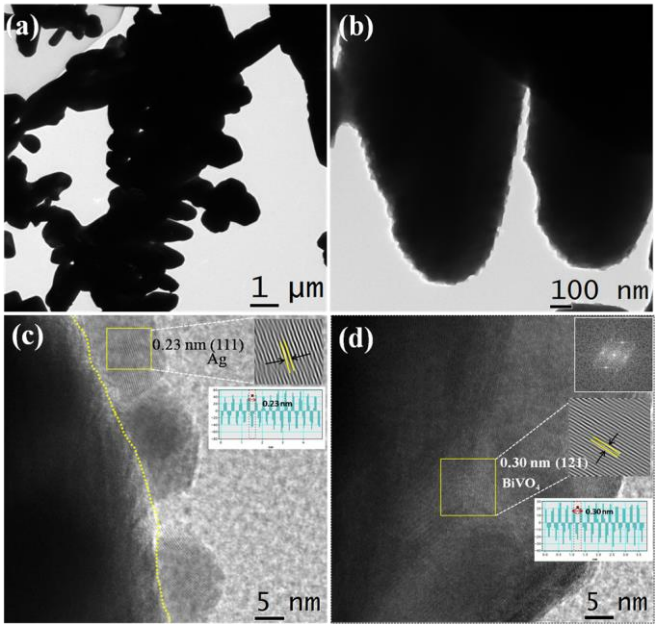

Fig. 3 (a, b) FETEM images of Ag:$BiVO_4$ and (c, d) HRTEM images of Ag and $BiVO_4$ respectively

The obtained Ag:$BiVO_4$ dendritic structure holds several key features such as interlinked connectivity through branched surfaces, propound effect of Ag nanocrystals, improved surface properties and stability. The incorporation of Ag into $BiVO_4$ structure leads to improved charge transfer kinetics on the surface and also facilitates the surface chemical reactions, which is expected to improve specific capacitance through establishing fast electron transfer channels during charge discharge process.[10,11] All these properties are extremely favorable for supercapacitor application.

Considering the unique dendrite structures of the present samples, we investigated the electrochemical performance of $BiVO_4$ and Ag:$BiVO_4$ in 6 M KOH electrolyte. The deviation in a cyclic voltammetry (CV) curve from ideal rectangular shape confirms pseudo-capacitive behavior of both materials as seen in Fig. 4a. It is further interesting to note that, for Ag:$BiVO_4$, the CV curve exhibits relatively high current density with well-defined redox peak, which is attributed to the improved

conductivity of Ag:$BiVO_4$ leading to better ionic and electronic conduction. For the $BiVO_4$ or Ag:$BiVO_4$ electrode, the capacitance mainly arises from the pseudocapacitance due to reversible redox transitions involving the insertion/extraction of protons and/or K^+ ions as well as the transitions between different valence state of V.[12] The possible reaction mechanism is expressed as follows:

$$BiVO_x + yM^+ + ye^- \leftrightarrow V_{2x-y}O_xM_y^{y+} \quad (M^+ = K^+ \text{ or } H^+) \qquad (1)$$

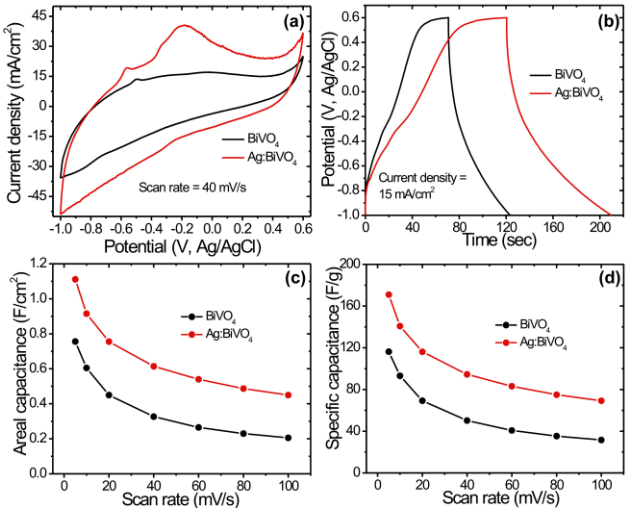

Fig.4 (a) CV curves and (b) Chronopotentiometry curves of $BiVO_4$ and Ag:$BiVO_4$ electrodes at scan rate of 40 mV/s and current density of 15 mA/cm^2, respectively (c) Variation of Areal capacitance of $BiVO_4$ and Ag:$BiVO_4$ nanostructures as a function of scan rates (d) Variation of specific capacitance as a function of scan rates

The CV curves at different scan rates for $BiVO_4$ and Ag:$BiVO_4$ are measured (see Fig. S.I.5). It is worth noting that as scan rate increases the area under the curve increases retaining redox peaks even at high scan rates suggesting excellent rate capability of this material. Fig. 4b shows galvanostatic charge/discharge (CD) curves of $BiVO_4$ and Ag:$BiVO_4$ samples at 15 mA/cm^2. Ag:$BiVO_4$ exhibits higher discharge time than $BiVO_4$ due to low internal resistance of Ag:$BiVO_4$, indicating improved conductivity of Ag:$BiVO_4$ (Fig. S.I.6). The CD curves for $BiVO_4$ and Ag:$BiVO_4$ samples at different current densities from 15 to 40 mA/cm^2 are provided in Fig. S.I.5. The CD curves show symmetrical nature even at high current densities, which further confirms high rate capability of Ag:$BiVO_4$ electrode. The preferable capacitor performance can be attributed to the improved electronic conductivity of the Ag:$BiVO_4$ derived from Ag coating. The above capacitor performance demonstrates that the $BiVO_4$ dendrites coated with Ag nanoparticles exhibit remarkable electrochemical performance for supercapacitor electrodes. The similar kind of improved electrochemical performance owing to improved conductivity of metals oxides coated with polypyrrole (PPy) polymers has been reported earlier.[13, 14] The improved conductivity of Ag:$BiVO_4$ is confirmed by electrochemical impedance measurements (see S.I.6).

For the quantitative analysis of the electrochemical performance, the specific capacitances were derived from the CV measurements. The areal and specific capacitances of $BiVO_4$ and Ag:$BiVO_4$ electrodes at different scan rate are shown in Fig. 4c and d, respectively. The maximum capacitances obtained for $BiVO_4$ and Ag:$BiVO_4$ are 0.75 F/cm^2 (116.3 F/g) and 1.12. F/cm^2 (170 F/g) respectively, at a scan rate of 5 mV/s. The high values of capacitance for Ag:$BiVO_4$ electrode can be attributed to the incorporation of Ag into $BiVO_4$ (improved conductivity) with unique 3D dendrite-like morphology. It is further interesting to note that, the capacitance retention is increased from 26 % to 32 % for Ag:$BiVO_4$ after the increase in scan rate from 5 mV/s to 100 mV/s. Further, the electrochemical stability of $BiVO_4$ and Ag:$BiVO_4$ is measured by charge/discharge cycles at 40 mA/cm^2 as presented in Fig. S.I.6. Both the $BiVO_4$ and Ag:$BiVO_4$ electrodes exhibit capacity retention in the range between 86-88 % after 4000 cycles. All of these results highlight the fact that the addition of Ag to $BiVO_4$ results in enhanced performance by facilitating the faradaic reactions.

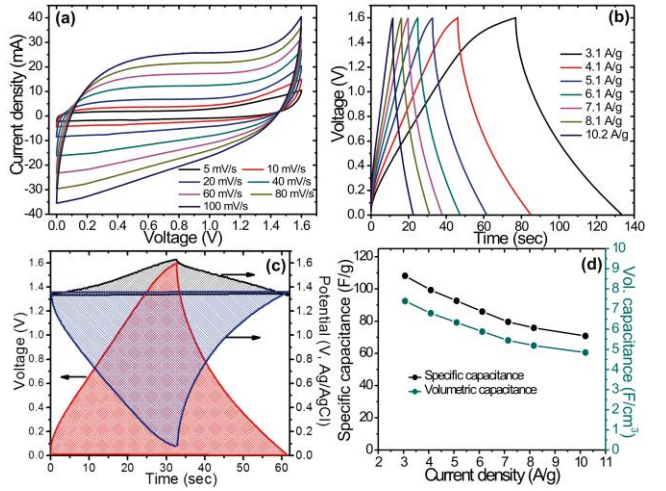

Fig. 5 (**a**) CV curves of Ag-$BiVO_4$ based symmetric cell at different scanning rates, (b) Galvanostatic charge/discharge (CD) curves of Ag:$BiVO_4$ based symmetric cell at different current densities (c) representative charge discharge cycle at 5.1 A/g for Ag:$BIVO_4$ symmetric cell (d) Variation of specific capacitance and volumetric capacitance at different current densities.

Strikingly, Ag:$BiVO_4$ electrode can work in wider potential window from -1.0 to 0.6 V (vs Ag/AgCl) as shown in Fig 4a and b). Taking advantage of wider potential window, we have assembled a symmetric cell based on Ag:$BiVO_4$ electrodes by sandwiching KOH-soaked separator in between. Thus, the Ag:$BiVO_4$ electrode can be used as both positive as well as negative electrode. Fig. 5a shows cyclic polarization curves of Ag:$BiVO_4$ symmetric cell at various scanning rates. Impressively, the cell can extend voltage window up to 1.6 V, beyond thermodynamic limit of water (1.23 V). It is further interesting to note that the CV curves retain rectangular shape even at high scan rates suggesting good rate capability of electrode materials. Furthermore, the galvanostatic charge/discharge (CD) curves were recorded at various current densities from 3.1 A/g to 10.2 A/g for Ag:$BIVO_4$ symmetric cell (Fig. 5b). It is worth noting that the Ag:$BIVO_4$ symmetric cell shows large voltage window of 1.6 V, which leads to an increased energy density. Fig. 5c shows a representative charge discharge cycle at 5.1 A/g for Ag:$BIVO_4$ symmetric cell.

Each electrode potential limit is also shown (black and blue curves on right Y axis). As expected charging and discharging branches are not straight lines due to the pseudocapacitive contribution. The positive and negative electrodes work in the voltage range: +1.35 to +1.6 V and +1.35V to +0.0 V. Therefore the voltage swing from the negative electrode is much larger than for the positive electrode.

Further, for the quantitative analysis of the electrochemical performance of Ag:$BiVO_4$ symmetric cell, the specific capacitance and volumetric capacitance of Ag:$BiVO_4$ symmetric cell were derived from the CV measurements (S.I.7). Fig. 5d shows the variation of specific capacitance and volumetric capacitance of Ag:$BiVO_4$ symmetric cell as a function of current densities. The Ag:$BiVO_4$ symmetric cell provides a high volumetric capacitance of 7.39 F/cm^3 (108.1 F/g for total mass of active material in both electrodes 4.9 mg/cm^2) at current density of 3.1 A/g. As expected, the capacitance decreases with increase in current density because of diffusion limitation caused by ionic motion of electrolyte. However, the volumetric capacitance at high current density of 7.1 A/g is still considerably high 5.44 F/cm^3 (79.5 F/g). It is noteworthy that the obtained volumetric capacitances are comparatively higher than that of some of the previously reported symmetric as well as asymmetric supercapacitors (see Table S2).[15-17,18] The areal capacitance at different current densities was also calculated and given in Fig. S.I.8. The maximum areal capacitance of 0.73 F/cm^2 was observed at current density of 20 mA/cm^2. The areal capacitance further decreases with increase in current density, consistent with that of volumetric capacitance.

Fig. 6a and b displays the Ragone plots of Ag:$BiVO_4$ symmetric cell. The maximum volumetric energy density of cell is found to be 2.63 mWh/cm^3 (38.43 Wh/kg) at power density of 167 mW/cm^3 (2.44 kW/kg). More interestingly, even at high power density of 558 mW/cm^3 (8.16 kW/kg), Ag:$BiVO_4$ cell exhibits energy density of 1.7 mWh/cm^3 (25.17 Wh/kg), confirming the great potential for application in high performance devices. The enhanced energy and power densities of Ag:$BiVO_4$ symmetric cell are ascribed to high conductivity of Ag:$BiVO_4$ electrode, unique dendrite-like architecture which provide extended voltage window. In comparison to recent novel sodium ion capacitors[19] (energy density of 98 Wh/kg at power density of 2.43 kW/kg), the gravimetric energy density of present Ag:$BiVO_4$ is smaller. However, the observed volumetric energy density is much higher than those of previous reports on symmetric and asymmetric supercapacitors which employed an aqueous electrolyte such as H-TiO_2@MnO_2 //H-TiO_2@C (0.30 mWh/cm^3, 5M LiCl)[18], Co_9S_8//Co_3O_4@RuO_2, (1.21 mWh/cm^3, 3M KOH)[21], VOx//VN (0.61 mWh/cm^3, 5M LiCl)[22], laser-scribed graphene (LSG)//LSG (0.09 mWh/cm^3, 1 M H_3PO_4)[17] demonstrating the remarkable capacitive behavior of Ag:$BiVO_4$/Ag:$BiVO_4$ in aqueous electrolytes.

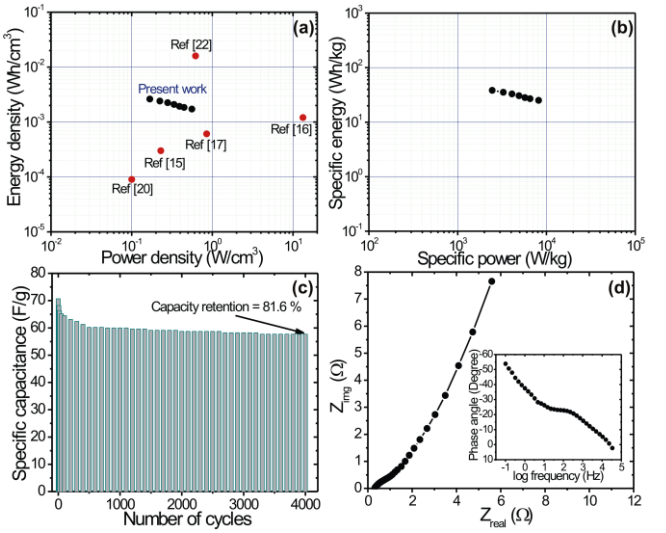

Fig. 6 (a, b) volumetric and gravimetric energy/power densities of Ag:$BiVO_4$ symmetric cell (c) Cycle performance of Ag:$BiVO_4$ symmetric cell, (d) Nyquist plots of Ag:$BiVO_4$ symmetric cell after 4000 cycles (Inset shows plot of phase angle with frequency)

The cycling stability is one of the most important features of high performance supercapacitor device. The stability of Ag:$BiVO_4$ symmetric cell was measured charge/discharge cycles at 10 A/g over 4000 cycles (Fig. 6c). The Ag:$BiVO_4$ symmetric supercapacitor retains 82 % of its initial capacitance after 4000 cycles which is higher than those of earlier reported systems composed of $BiVO_4$ asymmetric capacitor (42% after 200 cycles)[18] and VO_2//VO_2 symmetric supercapacitor (78.7 % after 4500 cycles)[20]. The improved cycling stability might be due to uniquely stable 3D hierarchical dendrite-like structure of Ag:$BiVO_4$. Fig. 6d depicts Nyquist plots of Ag:$BiVO_4$ symmetric cell showing very low ESR value (0.3 Ω) which suggests that the Ag:$BiVO_4$ have very small internal resistance with good ion response at high frequency ranges. The above results indicate that our Ag:$BiVO_4$ hybrid architecture based symmetric supercapacitor exhibits excellent electrochemical supercapacitive properties that could be due to a synergetic effect between noble metal Ag and nano-architectured $BiVO_4$. More importantly, assembling symmetric cells could eliminate the use of complex chemistries usually involved in asymmetric cells (different electrode materials) as well as complication in balancing charge (or mass) of both electrodes. Thus, Ag:$BiVO_4$ symmetric cell outclasses the high-voltage asymmetric counterparts under the same power and represents a noteworthy advance towards high energy density supercapacitors.

In conclusion, a novel Ag:$BiVO_4$ symmetric cell has been successfully fabricated for the first time demonstrating excellent supercapacitive properties. The cell offers an extended voltage window of 1.6 V which further leads to an excellent energy density of 2.63 mWh/cm^3 (38.63 Wh/kg) with high power density of 558 mW/cm^3 (8.1 kW/kg). In addition, notably, this symmetric cell exhibits significantly high volumetric capacitance of 7.39 F/cm^3 and good cycling stability (82 % retention after 4000 cycles). This successful strategy could be applied to the design of new symmetric

supercapacitors using noble metals for doping a variety of high-performing supercapacitor electrode materials.

Notes and References:

1 (a) F. Zhang, T. Zhang, X. Yang, L. Zhang, K. Leng, Y. Huang and Y. Chen, *Energy Environ. Sci.*, 2013, **6**, 1623., (b) D. P. Dubal, J. G. Kim, Y. Kim, R. Holze, C. D. Lokhande, W. B. Kim, *Energy Technol.* **2014**, *2*, 325., (c) D. P. Dubal, P. Gomez-Romero, B. R. Sankapal, R. Holze, *Nano Energy*, **2015**, 11, 377.

2 (a) P. Simon, Y. Gogotsi and B. Dunn, *Science (80-.).*, 2014, **343**, 1210., (b) D. P. Dubal, O. Ayyad, V. Ruiz and P. Gómez-Romero, *Chem. Soc. Rev.*, 2015, **44**, 1777., (c) M. M. Vadiyar, S. C. Bhise, S. K. Patil, S. A. Patil, D. K. Pawar, A. V Ghule, P. S. Patil and S. S. Kolekar, *RSC Adv.*, 2015, **5**, 45935..

3 (a) G. Yu, X. Xie, L. Pan, Z. Bao and Y. Cui, *Nano Energy*, 2013, **2**, 213., (b) J. Suarez-Guevara, V. Ruiz, P. Gomez-Romero, *J. Mater. Chem. A*, 2014, 2, 1014., (c) D. P. Dubal, R. Holze, P. Gomez-Romero, *Sci. Rep.*, 2014, **4**, 7349, (d) D. P. Dubal, J. Suarez-Guevara, D. Tonti, E. Enciso, P. Gomez-Romero, *J. Mater. Chem. A*, 2015, 3, 23483-23492

4 (a) F. Wang, S. Xiao, Y. Hou, C. Hu, L. Liu, Y. Wu, *RSC Adv.,* **2013**, 3, 13059, (b) D. P. Dubal, R. Holze, P. Gomez-Romero, *ChemPlusChem*, 2015, **80**, 944.

5 K. Xu, W. Li, Q. Liu, B. Li, X. Liu, L. An, Z. Chen, R. Zou and J. Hu, *RSC Adv.*, 2014, **2**, 4795..

6 A. Bello, F. Barzegar, D. Momodu, J. Dangbegnon, F. Taghizadeh, M. Fabiane and N. Manyala, *J. Power Sources.*, 2015, **273**, 305..

7 L-X. Ding, F-L. Zheng, J-W. Wang, G-R. Li, Z-L. Wang and Y-X. Tong, *Chem. Commun., 2012, **48**, 1275.*

8 R. Zou, Z. Zhang, M. F. Yuen, J. Hu, C. Lee and W. Zhang, *Sci. Rep.*, 2015, **5**, 1.

9 X. Sun, Z Firdoz, Ying-Xuan, E Li, L Lu, *Nanoscale*, 2013, **5**, 4379.

10 M. Sawangphruk, M. Suksomboon, K. Kongsupornsak, J. Khuntilo, P. Srimuk, Y. Sanguansak, P. Klunbud, P Suktha and P. Chiochan, *J. Mater. Chem. A*, 2013,**1**, 9630.

11 W. Lan, Y. Sun, Y. Chen, J. Wang, G. Tang, W. Dou, Q. Su and E. Xie, *RSC Adv.*, 2015,5, 20878.

12 (a) A. M. Engstrom, F. M. Doyle, *J. Power Sources*, 2013, 228, 120, (b) D. H. Nagaraju, Q. Wang, P. Beaujuge, H. N. Alshareef, *J. Mater. Chem. A*, 2014, 2, 17146, (c) X. Lu, M. Yu, T. Zhai, G. Wang, S. Xie, T. Liu, C. Liang, Y. Tong, Y. Li, *Nano Lett.*, 2013, 13, 2628

13 T. Qian, N. Xu, J. Zhou, T. Yang, X. Liu, X. Shen, J. Liang and C. Yan, *J. Mater. Chem. A,* 2015, **3**, 488

14 X. Zhang, X. Zeng, M. Yang and Y. Qi, *ACS Appl. Mater. Interfaces*, 2014, **6**, 1125.

15 X. Lu, M. Yu, G. Wang, T. Zhai, S. Xie , Y. Ling, Y. Tong and Y. Li, *Adv. Mater.* 2013, **25,** 267.

16 J. Xu, Q. Wang, X Wang, Q. Xiang, B. Liang, D. Chen and G. Shen, *ACS Nano*, 2013, **7**, 5453.

17 X. Lu, M. Yu, T. Zhai, G. Wang, S. Xie, T. Liu, C. Liang, Y. Tong, and Y. Li, *Nano Lett.* 2013, **13**, 2628.

18 Z. Khan, S. Bhattu, S. Haram, and D. Khushalani, *RSC Adv.*, 2014, **4**, 17378.

19 F. Wang , X. Wang , Z. Chang , X. Wu , X. Liu , L. Fu, Y. Zhu , Y. Wu and W. Huang, *Adv. Mater*. 2015, **27**, 6962

20 M. F. El-Kady, , V. Strong, , S. Dubin, and R. B. Kaner, *Science*, 2012, **335**, 1326.

21 X-J. Ma, W-B. Zhang, L-B. Kong, Y-C. Luo and L. Kang, *RSC Adv.*, 2015, **5**, 97239.

22 M. Acerce, D. Voiry and M. Chhowalla, *Nat. Nanotech.*, 2015, **10**, 313.